Accepted Manuscript

Multi-phase nature of sintered vs. arc-melted $Cr_XAlFeCoNi$ high entropy alloys - experimental and theoretical study

J. Cieslak, J. Tobola, J. Przewoznik, K. Berent, U. Dahlborg, J. Cornide, S. Mehraban, N. Lavery, M. Calvo-Dahlborg

PII: S0925-8388(19)32196-6

DOI: https://doi.org/10.1016/j.jallcom.2019.06.121

Reference: JALCOM 51019

To appear in: *Journal of Alloys and Compounds*

Received Date: 14 March 2019

Revised Date: 23 May 2019

Accepted Date: 10 June 2019

Please cite this article as: J. Cieslak, J. Tobola, J. Przewoznik, K. Berent, U. Dahlborg, J. Cornide, S. Mehraban, N. Lavery, M. Calvo-Dahlborg, Multi-phase nature of sintered vs. arc-melted $Cr_XAlFeCoNi$ high entropy alloys - experimental and theoretical study, *Journal of Alloys and Compounds* (2019), doi: https://doi.org/10.1016/j.jallcom.2019.06.121.

Multi-phase nature of sintered vs. arc-melted $Cr_xAlFeCoNi$ high entropy alloys - experimental and theoretical study

J. Cieslak[a*], J. Tobola[a], J. Przewoznik[a], K. Berent[b], U. Dahlborg[c] , J. Cornide[c], S. Mehraban[d], N. Lavery[d], M. Calvo-Dahlborg[c]

[a] *AGH University of Science and Technology, Faculty of Physics and Applied Computer Science, Al. Mickiewicza 30, 30-059 Cracow, Poland*
[b] *AGH University of Science and Technology, Academic Centre of Materials and Nanotechnology, Al. Mickiewicza 30, 30-059 Cracow, Poland*
[c] *GPM UMR6634, University of Rouen Normandie, Campus Madrillet, BP12, 76801 St-Etienne-du-Rouvray, France*
[d] *Department of Materials Science & Engineering, College of Engineering, Swansea University, Bay Campus, Fabian Way, Swansea SA1 8EN, UK*

*Corresponding author

Abstract

High entropy $Cr_xAlFeCoNi$ alloys with x= 0, 0.5, 1.0 and 1.5 were synthesized using arc-melting and sintering preparation techniques. Three crystal structures (*fcc*, *bcc* and σ) were observed using XRD technique, while EDX measurements showed the presence of up to three chemically different phases (FeCr-rich phase with *fcc* structure, AlNi-rich phase with *bcc* structure and Cr-rich phase with *bcc* and/or σ structures). The reasons for the observed phase coexistence were addressed to total energy electronic structure calculations using KKR-CPA method accounting for chemical disorder effects. Such theoretical analysis confirmed that the multi-phase system was energetically more favorable than the single-phase one. Furthermore, DSC measurements allowed to identify two phase transitions in melted samples, unlike sintered ones due to high-temperature nitrogen corrosion. This process turned out to be highly selective, resulting in the formation of the scales consisting of Al_nN_m–phases at the cost of total Al loss in the HEA alloy.

1. Introduction

High Entropy Alloys (HEA) or multi-major component alloys are a new concept of alloys which have been under development since 2004 [1,2]. The use of only major elements in their composition opens up a new field in metallurgy with an increasing number of publications devoted to their potential properties and applications, as well as to their design and characterization [3]. Although it was first suggested that HEA are single-phased due to their usual diffraction patterns mostly recorded by standard X-ray, it is now well established that most of HEA with minimum 5 elements are single structure for some domains of *e/a* and multi-phased [4,5]. The identified structures in HEA are *fcc*, *bcc* and *hcp*. The participation of individual phases leads to the control of the properties, especially mechanical [6-10].

Among the most investigated systems is Co-Cr-Fe-Ni-Al, which has attracted a lot of interest for the following reasons:

- The system presents transitions from *fcc* to *bcc* when the amount of some elements, e.g. Al, is varied [6-9,11-13].

While some studies on the Co-Cr-Fe-Ni-Al system have looked at the influence of Fe and Ni on the structure and properties, the impact of Cr has not been reported. In this work we present a comparative study of alloys of $Cr_xAlFeCoNi$ composition produced by two different techniques.

2. Materials and methods

2.1. Sample preparation

Two series of samples differing by synthesis methods have been prepared. Each series consisted of four samples of $Cr_xAlFeCoNi$, with variable Cr content (x= 0, 0.5, 1 and 1.5). Purities of the used ingredients as well as granulations of the used powders are indicated in Table 1.

Table 1: Purities and granulations of elemental powders used for sample preparation.

Element	Fe	Cr	Co	Ni	Al
Purity [%]	99.9	99.2	99.8	99.9	99.5
Granulation	< 7μm	< 7μm	1.6μm	3-7μm	7-15μm

One series of alloys (SM) was prepared by melting a mixture of pure elements in an arc-furnace under an argon atmosphere. Each sample was re-melted four times inverting the ingot each time to improve the melting homogeneity. The mass of each sample made this way was only ~5g and the cooling of the droplets from the melting temperature (~1400°C) to ambient temperature took no longer than a minute. Consequently, it can be assumed that the element distribution in the prepared samples corresponds to an equilibrium state near the melting temperature. The alloys were subsequently annealed at 1000°C in vacuum of $6 \cdot 10^{-6}$ mbar for 72 hours and quenched on a thick brass plate.

The second series of alloys (SS) was prepared by sintering a blended mixture of pure metallic powders. The powders were mixed in appropriate amounts and then compressed. The obtained pellets were pre-annealed at 500°C for one day and subsequently annealed at 1000°C for 2 weeks in a vacuum of $6 \cdot 10^{-6}$ mbar. Finally, the samples were quenched on a brass plate whilst still under vacuum. This two-step procedure of annealing and cooling was carried out in order to avoid possible Al loss from the sample.

At this stage it should be noted that both types of samples have been homogenized at 1000°C: the SM ones for 72 hours in the as-cast state, the SS ones for 2 weeks from as-compacted powders.

2.2. Experimental details

Microstructure observations and chemical analyses were carried out in a FEI Versa 3D scanning electron microscope equipped with an EDAX Apollo XP energy dispersive X-ray spectrometer (EDX), operated at 20 kV accelerating voltage.

Thermal and gravimetric characterizations of the alloys were made on a Netzsch STA 449C calorimeter. The measurements were performed under nitrogen atmosphere at the rate of 30 K/min during both the heating and subsequent cooling cycles.

The powder XRD patterns were collected at ambient temperature with a PANalytical Empyrean diffractometer using a diffracted beam graphite monochromator and an X'Celerator

terms of lattice parameters and common line widths. It was also assumed, that for *fcc* and *bcc* phases each crystallographic position was occupied by all constituent elements, with probabilities corresponding to the compositions of the phases as determined by EDX measurements. For the σ-phase, common occupancy corresponding to the co-existing *bcc* phase was used.

3. Computational details

Electronic structure calculations of disordered $Cr_xAlFeCoNi$ ($0 \leq x \leq 1.5$) HEA alloys assuming both fcc and bcc crystal structures were performed with the use of the charge- and spin-self-consistent the Korringa-Kohn-Rostoker method employing the coherent potential approximation (CPA) [26,27] in order to account for chemical disorder. The CPA model allows to treat random atoms distribution on selective sites (only one site in considered *fcc/bcc* alloys) via construction of the effective medium, which is defined by the averaging of Green's functions ascribed to particular atoms, G_i, over their concentrations, x_i, i.e. $G_{cp} = \Sigma x_i G_i$ (i=Fe, Cr, Co, Ni and Al). The CPA condition is solved in self-consistent way. As the CPA model does not rely on simple averaging of physical properties of atoms constituting disordered alloy, it is not always easy to correlate the properties of the alloy resulted from KKR-CPA calculations, with the respective properties of the elemental compounds, especially in such disordered multi-atom system. As above-mentioned and it is really worth noting that within the CPA model, the symmetry of the unit cell is maintained in the whole range of alloy composition, for which ground state properties can be computed (e.g. density of states, magnetic moments, total energy contributions) and then compared for different alloy compositions.

In the case of HEAs the total energy obtained from KKR-CPA code was converged below 1 meV. In both investigated phases the equilibrium lattice parameter was determined from the minimum of the total energy as obtained from a parabolic fit to the calculated values, for which the electronic structure and ground state properties were next computed. The self-consistent crystal potential was prepared within the local density approximation (LDA) framework, using the Perdew-Wang formula for the exchange-correlation part [28].

The KKR-CPA computations in disordered HEA have been restricted to only the spherical part of the potential (muffin-tin) with truncations on each atom up to the angular momentum cutoff l_{max} = 3. For well-converged atomic charges (below $10^{-3}e$) and crystal potentials (below ~10meV), the total, site-decomposed and *l*-decomposed, density of states (DOS) were computed using the integration tetrahedron method in reciprocal space and 560 *k*-space points in the irreducible part of the Brillouin zone. The total magnetic moment per Wigner-Seitz cell and all atomic magnetic moments inside muffin-tin spheres were calculated. The Fermi level, E_F, was accurately determined from the Lloyd formula [29]. In our KKR-CPA computations both core and valence states of electrons were treated in a nonrelativistic approach.

It should be highlighted that our KKR-CPA calculations were performed for the nominal HEA systems as well as for the phases identified from EDX measurements. Since the combined results of XRD (structure sensitive) and EDX (composition sensitive) refinements do not allow correlation of detected structures to detected compositions, all computations were carried out for both *bcc* and *fcc* structures. Consequently, the comparison of total energies obtained for different structure alternatives and the total energy calculated for the nominal composition provides a basis for discussion of the relative crystal stability.

Both the SM and the SS samples were investigated by Differential Scanning Calorimetry (DSC) and by Thermal Gravimetric Analysis (TGA). The curves measured during heating and subsequent cooling are shown in Figs 1 and 2. All curves show some oscillations and the temperatures at which the most prominent features are seen are listed in Tables 1 and 2. During heating all the SM samples pass phase transformations around 600 and 1000°C, even if both only can be seen as hints for the x=0 sample. Similar features have earlier been seen in equimolar (x=1) as-cast samples [12,14,20]. The temperature of the first distinct transformation that does not change with increasing Cr content and might correspond to the phase transformation observed by [14] at about 630°C in an equimolar alloy which is partly of magnetic origin. It is conceivable that this feature corresponds to the ones seen at the somewhat lower temperatures in the cooling curves. The transformation is thus at least partly reversible and it might correspond to a composition-dependent peritectic phase transformation. Another feature obviously irreversible is seen in 1000-1200°C temperature range, more distinct and moving to lower temperatures with increasing x value. A similar feature has also previously been observed and suggested to be connected to a sigma-phase decomposition [20]. The onsets of melting and solidification are varying with alloy composition indicating different phase compositions for the different alloys.

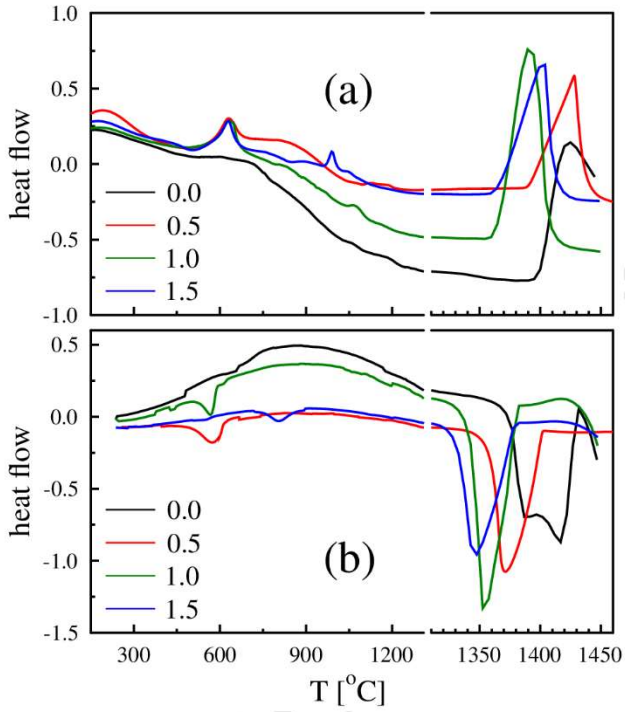

Fig.1 Measured DSC curves for $Cr_xAlFeCoNi$ alloys produced by arc melting (SM series) during a) heating and b) subsequent cooling.

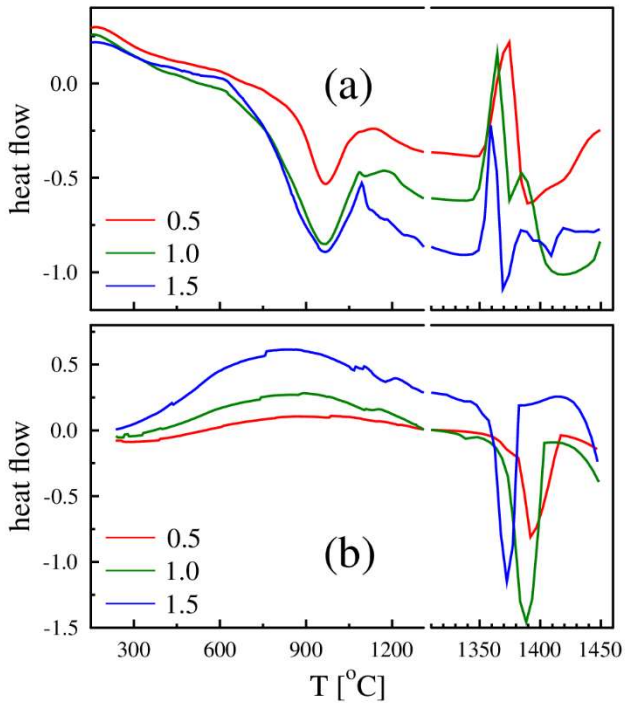

Fig. 2 Measured DSC curves for $Cr_xAlFeCoNi$ alloys produced by sintering (SS series) during a) heating and b) subsequent cooling.

The DSC curves measured for the SS alloys have a substantially different shape than the ones measured for the SM alloys. The curves indicate that a continuous ordering takes place in the alloys during heating up to about 900°C which is followed by a phase transformation at about 960°C (see table 2) independent of alloy composition. Other features in the DSC curves do neither vary much with alloy composition. However, the shape of melting peaks indicates a two-phase composition of all alloys which is not present on the following solidification.

Table 2. Temperatures (°C) at which features are seen in the DSC measurements on $Cr_xAlFeCoNi$ alloys produced by arc melting (SM).

x	Heating			Cooling		
	1st feature (peak) (°C)	2nd feature (peak) (°C)	Onset of melting (°C)	Onset of solidification (°C)	1st feature (peak) (°C)	2nd feature (peak) (°C)
0	~700	~1180	1399	1432	-	~680
0.5	630	~1150	1391	1403	-	576
1.0	630	1065	1364	1382	-	567
1.5	630	990	1362	1378	805	~550

Table 3. Temperatures (°C) at which features are seen in the DSC measurements on $Cr_xAlFeCoNi$ alloys produced by sintering (SS).

	Heating	Cooling

1.5	965	1351	1369	1383

4.2. Microstructural and chemical analyses

Compositions of individual phases were estimated using SEM-EDX measurements. EDX linescans were used to identify any changes of elemental composition along a line. For SM series, annealing of the Cr-containing samples at 1000°C resulted in a decomposition into two or three phases (Fig. 3a). In all cases similar dendritic structures were observed. The size of the individual phases did not exceed 2-3 μm. For the investigated SM samples phase compositions were determined. The results are presented in Fig. 4a-c. Three kinds of phases were found in all cases, below discussed as FeCr-rich (the brightest phase), Cr-rich (intermediate grey phase) and AlNi-rich (the darkest phase). Results of EDX analysis are shown in Table 4.

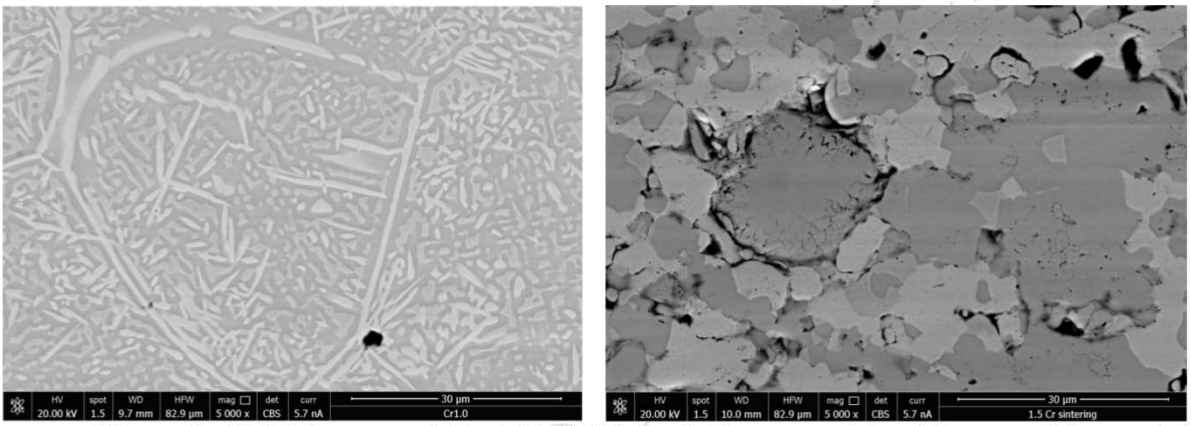

Figure 3: SEM images of $Cr_xAlFeCoNi$ (x=1.0) prepared by (a) arc-melting and (b) sintering methods.

Table 4. Phase compositions (at%) of $Cr_xAlFeCoNi$ phases (FCC_B, BCC_D and BCC_G) for two series of samples (SM and SS) as detected from EDX measurements.

x	SM														
	FeCr-rich (FCC_B)					AlNi-rich (BCC_D)					Cr-rich (BCC_G)				
	Cr	Al	Fe	Co	Ni	Cr	Al	Fe	Co	Ni	Cr	Al	Fe	Co	Ni
0.0	-	-	-	-	-	0	21.5	26.1	26.9	25.5	-	-	-	-	-
0.5	16.1	11.0	29.9	25.7	17.3	5.3	29.5	15.6	21.7	28.1	-	-	-	-	-
1.0	24.3	8.5	27.5	24.4	15.3	9.4	29.3	13.8	19.9	27.6	37.9	6.3	26.5	19.8	9.5
1.5	35.9	7.3	22.4	20.1	14.3	13.5	29.6	12.7	17.7	26.5	46.4	3.4	23.4	19.4	7.4
	SS														
0.0	-	-	-	-	-	0	23.1	26.2	25.1	25.6	-	-	-	-	-
0.5	20.5	5.7	35.6	24.5	13.7	4.8	30.3	15.6	19.6	29.7	-	-	-	-	-
1.0	27.7	5.1	30.8	23.2	13.2	6.9	31.1	12.8	18.3	30.9	44.1	3.9	30	15.9	6.1
1.5	28.6	5.0	28.4	24.3	13.7	30.1	7.8	11.9	18.3	31.9	43.3	5.8	25.3	18.0	7.6

As is seen in Fig. 3b the observed phases coexist in a quite different way in the SM samples as compared to the SS ones. In the latter, they are forming large (20-40μm) grains, whose

a certain amount of macroscopic pores, with sizes and distributions which correspond to those visible in the samples before annealing.

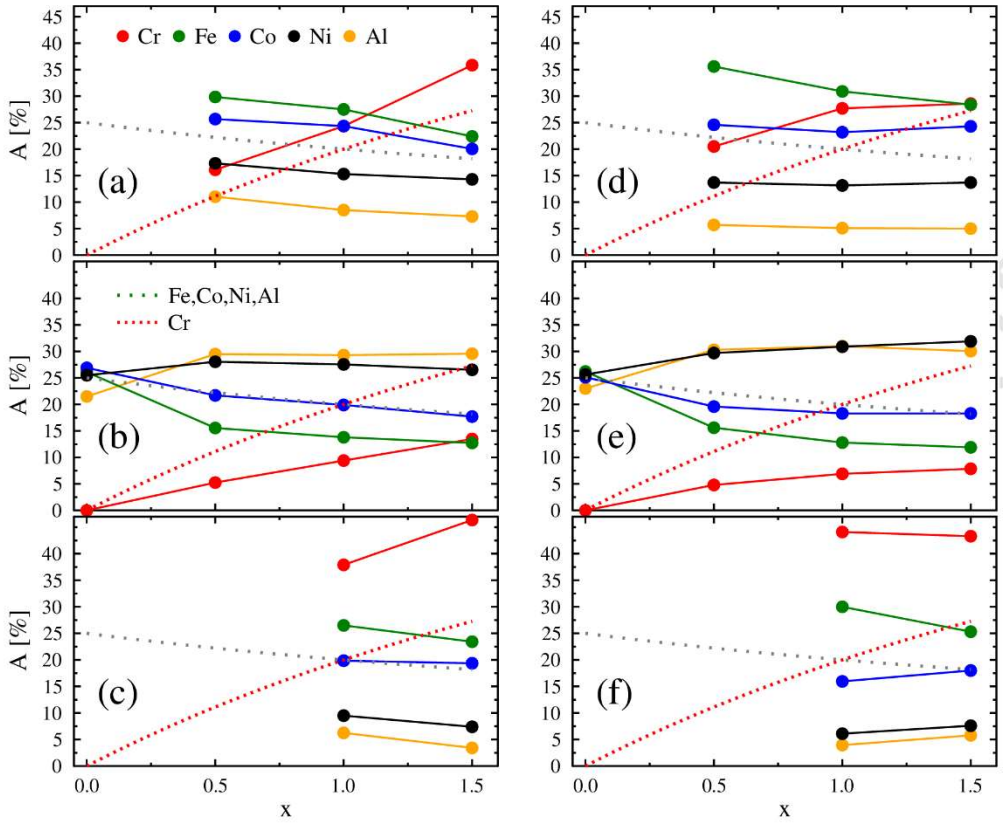

Figure 4: (Color online) Concentrations of elements in (a) FCC_B-phase, (b) BCC_D-phase and (c) BCC_G-phase, for the SM series. See Table 3. Dashed/dotted lines stand for the nominal concentration of Cr/other elements. Corresponding results obtained for the SS series are presented on (d-f).

Interestingly, comparing the samples with various Cr contents within the same series (SM or SS), it can be noted that the composition of each of detected phases only slightly changes with increasing the value of *x*. The most pronounced variation in all phases can be observed for Cr content, whereas the concentrations of remaining elements vary in a much narrower range.

On the whole, accounting for apparent similarities of phase compositions of HEA obtained using two completely different preparation methods (sintering against arc-melting) one can conclude that the proposed sintering technique of pure metallic powders well reproduces results of traditional arc-melting technique, and also gives the unique opportunity to investigate relatively large areas of distinct phases.

4.3. XRD measurements

In all samples, both melted and sintered, single *bcc* or coexistence of *bcc*, *fcc* and σ phases, were observed. The texture present in the melted samples hinders proper analysis of the

alloys belong to so-called Domain II with *bcc* phases, and for x=1.0 and 1.5, they belong to Domain II with mixed phases, σ, etc. Their lattice parameters are presented in Table 5. As one can see, they only slightly depend on the nominal Cr concentration which stays in line with the fact, that stoichiometries of particular phases do not considerably change. The σ-phase lattice parameters are close to those of σ-FeCr*X*, *X*=Co, Ni [30]. The presence of the σ-phase significantly impedes unique analysis of diffractograms, because of unknown sublattice occupancies. Finally, on the basis of the measured diffraction pattern, one can determine the percentage of each phase (Table 4 and Fig. 6a), but their contributions can only be roughly estimated due to unknown sublattice occupancies in the σ-phase.

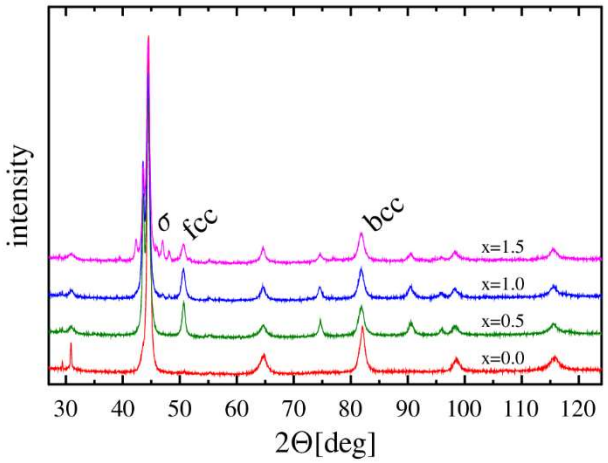

Fig. 5 XRD diffraction patterns for the SS series of $Cr_xAlFeCoNi$ alloys with various x.

As it was already mentioned, in the $Cr_xAlFeCoNi$ HEA system the σ-phase was detected for $x \geq 1$. Its stoichiometry has been determined for the equimolar system [19] and its abundance increases with Cr nominal content. This phase is known to appear in various intermetallic systems, but always as a result of annealing at elevated temperatures. Since the stoichiometry of the detected σ-phase is very similar to Cr-rich one, it can be assumed that the transformation process from Cr-rich phase to σ-phase occurs during long isothermal annealing. Unfortunately, sublattice occupancies of the resulting structure are unknown.

On the basis of previous findings [19] three chemically different phases can be assigned to the two (or three) detected crystallographic structures. And so, FeCr-rich phase has *fcc* structure, called there FCC_B (see Table 4), AlNi-rich phase has *bcc* structure called BCC_D, whereas Cr-rich phase can be detected as both BCC_G and σ phases. As it follows from such assignments, one cannot characterize the system in a unique way, since two crystalline phases (BCC_D and BCC_G) cannot be separated using the standard XRD technique, and at the same time BCC_D and σ phases have very close chemical compositions.

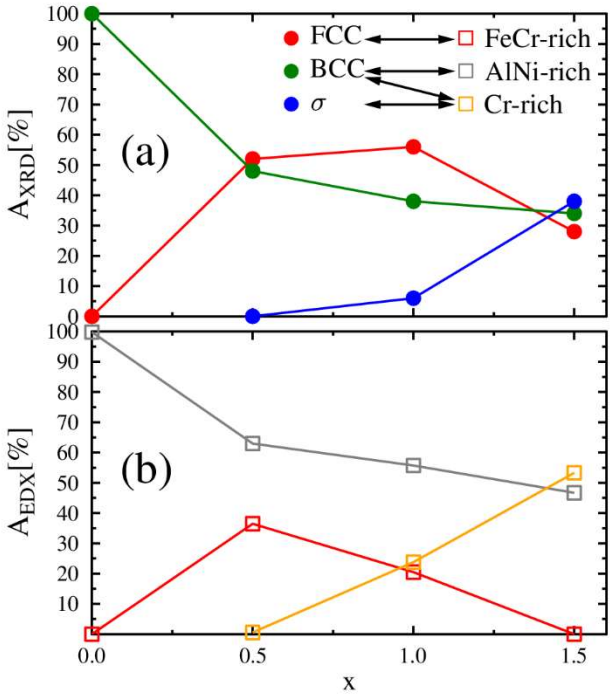

Fig. 6 (Color online) Amounts of various phases for the SS $Cr_xAlFeCoNi$ alloys with different Cr content, *x*, as determined using (a) SEM-EDX (at%) and (b) XRD techniques (vol%) . Lines added as a guide to eyes.

The stoichiometry of the phases present in a sample and the knowledge of its nominal composition allow to determine the actual phase composition of this sample based on EDX measurements, only. It can be done, by minimizing the summation value

$$\sum_j \left(\sum_i p_i \, x_{ij} \; - \; n_j\right)^2 \qquad (1)$$

where p_i denotes the amount of *i*-th phase, x_{ij} stands for the concentration of *j*-th element in the *i*-th phase and n_j - the nominal concentration of element *j* (see Table 4). Such calculations were performed for the SS series, and the results are shown in Fig. 6b for all detected phases. Unfortunately, it is not possible to directly compare the results obtained using these two techniques, since two present *bcc* structures cannot be distinguished using XRD-technique on one hand, as well as BCC_G and σ phases are very similar in EDX technique on the other hand.

4.4. Electronic structure KKR-CPA calculations

It is widely accepted that the relative stability of crystal phases can be analyzed using the Gibbs free energy (*G=E-TS*) directly depending on total energy *E* of a system and all entropy contributions (electronic, phonon, magnetic and configuration) scaled with temperature (*TS*). In the case of HEA systems, the configuration entropy seems to be the key factor responsible for minimization of *G*. It should be recalled that the configuration entropy of the crystalline *n*-component system with randomly distributed elements, S_{conf}, is maximal for the equal concentrations of constituting elements. In consequence, the total S_{conf} always decreases when the system decomposes into two or more different phases. As the integrated *G*-values of all subsystems (different phases) is smaller than the corresponding *G*-value of the single phase

concentrations of constituents (randomly distributed on lattice sites) corresponding to the nominal alloy compositions for both *fcc* and *bcc* structures and the computed energies are called here $E(x)^{nom}{}_{fcc}$ and $E(x)^{nom}{}_{bcc}$, respectively. Considering however, that the experimentally investigated alloys are mostly multiphased, the KKR-CPA calculations were also performed for all determined phases (with actual stoichiometry and also assuming both crystal structures).

Since the σ-phase has much more complicated structure (five elements distributed over five sites of the tetragonal unit cell, with different probabilities), and its presence is generally caused by annealing rather, than formation during solidification of the system, the KKR-CPA calculations for this phase were not yet performed.

Lattice parameters analysis

For all above-mentioned phases the equilibrium lattice constant was obtained from the total energy minimization. The results are presented in Fig. 7 and compared to the experimental values (Table 5). As expected from the well-known LDA limitations, the calculated lattice parameters are smaller than the experimental ones, measured at RT. However, the comparison of the calculated lattice parameters of the nominal and decomposed phases is more important. As one can clearly see, the unit cell of the FCC_B-phase is larger than that of the nominal *fcc*, while BCC_D and BCC_G-phases are very similar and apparently smaller than the nominal one. The latter theoretical result remains in line with the fact that the observed two *bcc* phases are indistinguishable using standard XRD diffraction techniques.

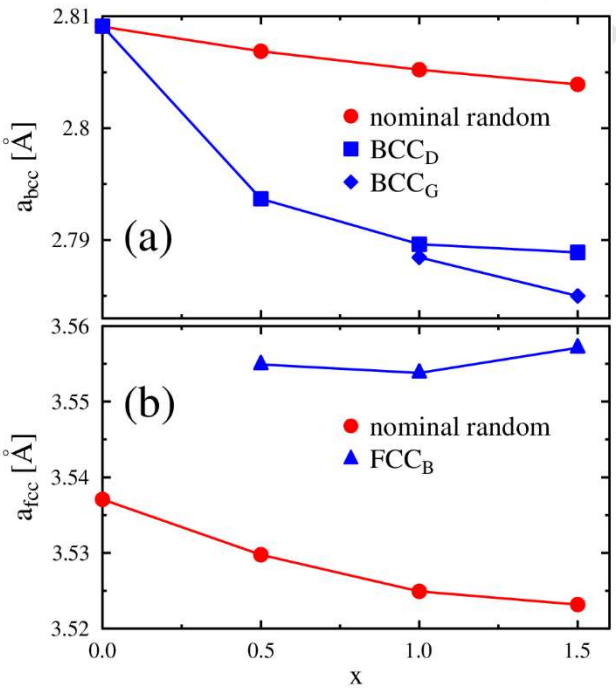

Fig. 7 (Color online) Variation of lattice parameters of (a) *bcc* and (b) *fcc* phases for the $Cr_xAlFeCoNi$ alloys with Cr content *x* as determined from the KKR-CPA calculations.

Table 5: Lattice parameters of *bcc* and *fcc* phases detected in SS samples, determined from XRD measurements

x	a_{fcc} [Å]	a_{bcc} [Å]
0.0	-	2.8775(1)
0.5	3.5965(2)	2.8825(1)
1.0	3.5992(2)	2.8828(1)
1.5	3.5987(2)	-

Relative crystal stability

Calculated total energy values of the hypothetical phases with nominal compositions $E(x)^{nom}{}_{fcc}$ and $E(x)^{nom}{}_{bcc}$ were compared to the total energies of the decomposed subsystems, taking into account all occurring phases, according to Eq. (1)

$$\Delta E = \sum_i E_i x_i - E_{bcc}^{nom} \qquad (2)$$

where E_i denotes the total energy of the i-th phase and x_i stays for its contributions.

It is worth noting that the differences between $E(x)^{nom}{}_{fcc}$ and $E(x)^{nom}{}_{bcc}$ are relatively small (less than 5 meV) for all Cr concentrations and therefore ΔE is presented with respect to $E(x)^{nom}{}_{bcc}$ only. As it can be seen from Fig. 8, for all analyzed compositions ΔE-values are negative, and so all decomposed systems are more stable than the nominal ones. The calculated energy difference ΔE decreases with nominal Cr concentration, which may indicate that increasing Cr content tends to promote multi-phase system against the single phase one. Moreover, in view of the KKR-CPA total energy analysis, it appears that the SS samples (sintered) appear to be more stable than the corresponding SM samples (melted and annealed). Such theoretical conclusion seems to be coherent with the fact that the sintered samples were homogenized much longer than the annealed ones, hence they are closer to the equilibrium state.

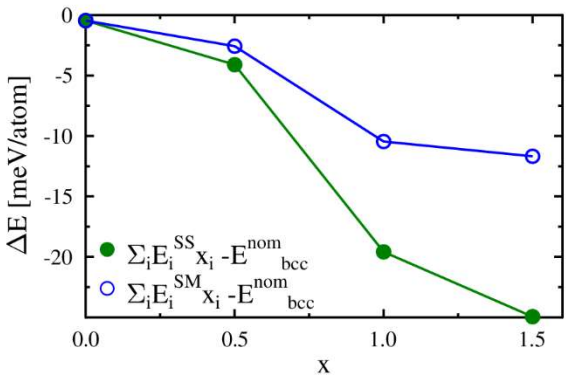

Fig. 8 (Color online) Energy differences between multiphase systems for various Cr content, x, and corresponding hypothetical *bcc*-phase as determined using electronic structure calculations.

4.5. High temperature nitrogen corrosion

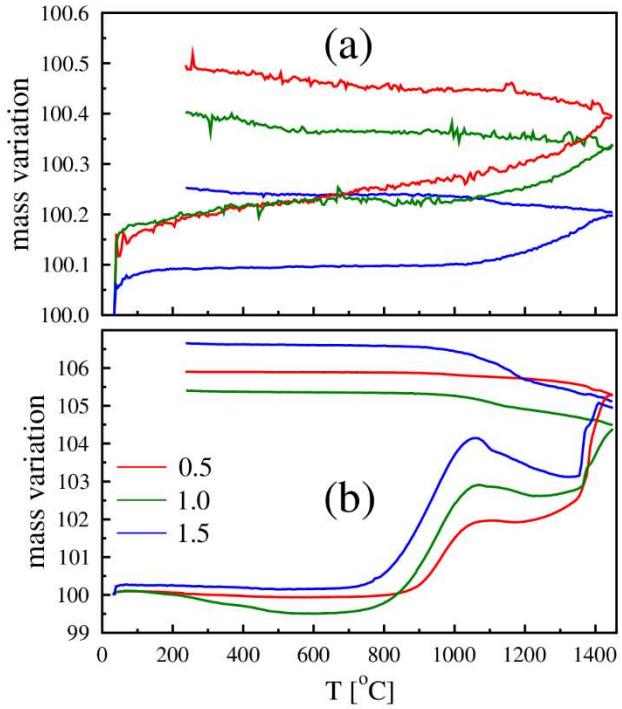

Fig. 9: Thermogravimetric curves measured for the $Cr_xAlFeCoNi$ alloys produced by a) arc melting (SM series) and b) sintering (SS series) during heating and subsequent cooling.

During the thermogravimetric (TGA) measurements it was found that the weight of both the SM and the SS alloys increased (see Fig. 9). This was observed during heating and cooling. The oxygen content of the flow gas was very small and it could be concluded that the weight increase was due to nitrogen absorption. The effect seen for the SM alloys was smaller than that observed for the SS alloys, probably due to their porous microstructure. For both series of alloys, the absorption process started during heating at about 800°C and continued up to the melting point. After solidification and during the subsequent cooling the process proceeded but at a slower rate.

The XRD pattern measured for the equimolar SM alloy after cooling to ambient temperature showed that the absorption of nitrogen resulted in an increase of the lattice constant of the *fcc* lattice from 3.578Å to 4.085Å. It can be concluded, within the accuracy of the XRD measurement, that nitrogen atoms are incorporated into interstitial positions without significantly changing the crystalline structure, since the unit cell only expands. This phenomenon has earlier been observed for e.g. nitride films that have been exposed to nitrogen gas at different temperatures and pressures [31-33].

As can be seen in Fig. 9, the SS alloys absorb a large amount of nitrogen during heating and also during the subsequent cooling. The absorption process starts at about 800°C and it is followed by a second one during the alloy melting. The start of the second process corresponds closely to the melting temperature as can be seen in DSC Fig. 2. The nitrogen

type (a=3.107Å, c=4.972Å). Small amounts of two *fcc* structures seem also to be present, one with a lattice constant equal to about 3.59Å and one with a lattice constant of about 4.12Å. These lattice parameters correspond closely to the one of the hexagonal AlN phase [33], the *fcc* structure of the CoCrFeNi alloy [4] and the *fcc* structure measured for the arc-melted and annealed equimolar CoCrFeNiAl alloy mentioned above.

The crystal structure of SM alloys with x=1 and 1.5 are considerably more complex and it is not possible to uniquely derive their structural details from the measured XRD patterns because of overlap and asymmetries of diffraction peaks. A profile refinement does not give convincing results. It is though very probable that the x=1.5 alloy contains a *hcp* structure with a=2.95Å, c=3.50Å, probably a *fcc* structure with a=4.08Å (maybe the same structure as seen in the equimolar SM alloy) and a small amount a *fcc* structure with a=3.58Å. Some more structures corresponding to some few unindexed peaks probably also exist in the alloys. It can be mentioned that because of the large Cr content one might expect to find CrN or Cr_2N but these phases seem not to be present.

EDX analyses of SS samples carried out after DSC measurements showed that their morphology has changed and two phases were detected: the bright one, not containing Al and the dark one, mainly consisting of Al and N elements (see Fig. 10). The dark phase occurs at the grain boundaries, corresponding to the size and morphology of grains already present in SS samples before DSC measurements (compare Fig. 10-a and 10-b). The compositions of the two phases are shown in Table 6. Fig. 11 presents the phase compositions of the bright phase versus Cr nominal content. As can be noticed, the stoichiometry of bright phase grains corresponds to the $Cr_xFeCoNi$ single-phase system, while the dark areas to the average composition of Al_5N_2.

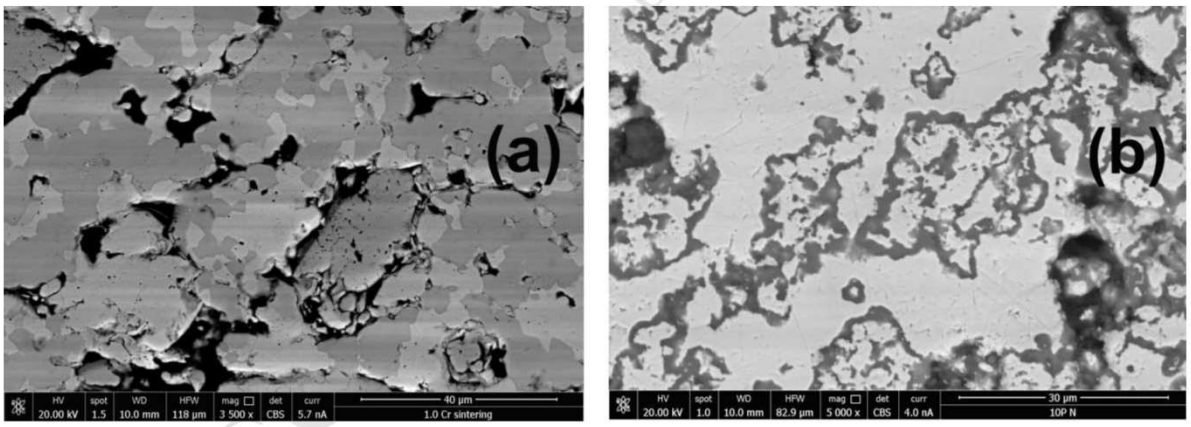

Fig. 10. SEM images of the SS equimolar alloy taken at ambient temperature (a) before and (b) after the DSC measurement.

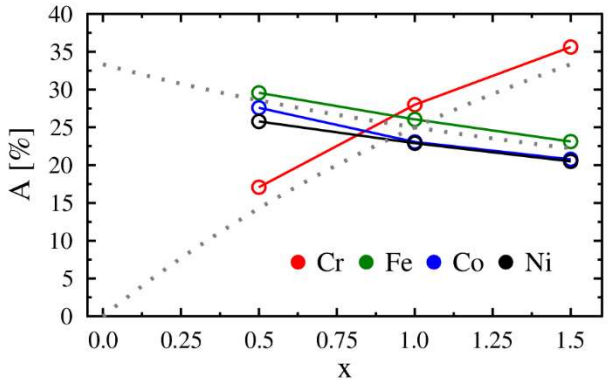

Fig. 11. Phase compositions of the SS $Cr_xAlFeCoNi$ bright phase as determined by EDX after the DSC measurements.

Table 6. Elemental compositions of the SS $Cr_xAlFeCoNi$ phases, as determined by EDX and XRD after the DSC measurements.

x	bright phase					dark phase		
	Cr [at%]	Fe [at%]	Co [at%]	Ni [at%]	a [Å]	Al/N	a [Å]	c [Å]
0.5	17.1	29.6	27.6	25.8	3.59/4.12	2.43	3.107	4.972
1.0	28.0	26.1	23.1	22.9	3.58/4.08	2.55	2.95	3.50
1.5	35.7	23.1	20.8	20.5		1.97		

Based on the experimental results, one can conclude that in the $Cr_xAlFeCoNi$ system over 900°C nitrogen corrosion has occurred. This was a selective process, which in practice relied on the removal of Al atoms from the host and formation of scale layers mainly composed of Al and N. Such phenomenon was favored by a large effective surface of the sample due to the preparation method resulting in large number of pores after sintering (unlike the arc-melted samples). In consequence, a pattern of grains of the Al-free HEA alloy, surrounded by scale layers composed of aluminum nitride, was formed in the sample (Fig. 10a,b). The stoichiometry of these layers was determined on the basis of EDX measurements. Since the thickness of the dark phase scales is relatively small, the electron beam can also excite the atoms of the areas well below the surface of the sample and therefore the measured signal may also contain some contributions from the bright phase. For this reason, only the average ratio of the Al and N concentrations (generally producing 80-90% of the signal) is presented in Table 5, which corresponds to the ratio of these elements in the scale (the bright phase does not contain Al nor N). The ratio values correspond to the stoichiometry of the Al_5N_2 or Al_2N phases, but they seem to be the values related to the averaged content of Al and N in different possible clusters in the Al_nN_m system [34,35].

Conclusions

Two series of high entropy $Cr_xAlFeCoNi$ alloys with variable chromium content were synthesized using arc-melting (SM series) and sintering (SS series) preparation techniques. Structural studies (XRD) revealed the (co-)existence of three phases with *fcc*, *bcc* and σ structures, while EDX measurements showed the presence of up to three chemically different phases, similiar for SM and SS series. They were identified as FeCr-rich phase with *fcc*

for the observed phase separation in the $Cr_xAlFeCoNi$ HEA system was addressed to total energy electronic structure calculations using KKR-CPA method, which enables to account for chemical disorder effects. Comparison of E_{tot} of nominal HEA compositions with the sum of E_{tot} of experimentally detected phases (averaged over their contributions), evidently showed that the multi-phase system was energetically more favorable than the single-phase one. DSC measurements performed on SM samples allowed to identify two phase transitions at temperatures ~630 °C and ~1100 °C. Conversely, such transitions were not observed for SS samples, due to high-temperature nitrogen corrosion. This process turned out to be highly selective, resulting in the formation of the scales consisting of Al_nN_m–phases at the cost of total Al loss in the HEA alloy.

Acknowledgements

This work was supported by the National Science Centre in Poland (Grant UMO-2015/17/B/ST3/01204) and the AGH UST statutory tasks (No. 11.11.220.01/3 and 5) from the Polish Ministry of Science and Higher Education.

References

[1] J.W. Yeh, S.K. Chen, S.J. Lin, J.Y. Gan, T.S. Chin, T.T. Shun, C.H. Tsau, S.Y. Chang, Nanostructured high-entropy alloys with multiple principal elements: Novel alloy design concepts and outcomes, Adv. Eng. Mater. 6 (2004) 299–303.

[2] B. Cantor, I.T.H. Chang, P. Knight, A.J.B. Vincent, Microstructural development in equiatomic multicomponent alloys, Mater. Sci. Eng. A 375-377 (2004) 213-218.

[3] M.C. Gao, J.W. Yeh, P.K. Liaw, Y. Zhang. High-Entropy alloys: Fundamentals and applications. eds, Springer, 2016.

[4] U. Dahlborg, J. Cornide, M. Calvo-Dahlborg, T. Hansen, A. Fitch, Z. Leong, S. Chambreland, R. Goodall. Structure of some CoCrFeyNi and CoCrFeNiPdx multicomponent HEA alloys by diffraction techniques. J. Alloys and Compounds 681 (2016) 330-341.

[5] M. Calvo-Dahlborg, S.G.R. Brown. Hume-Rothery for HEA classification and self-organizing map for phases and properties prediction. J. Alloys and Compds 724 (2017) 353-364.

[6] Y.F. Kao, T.J. Chen, S.K. Chen, J.W. Yeh. Microstructure and mechanical property of as-cast, -homogenized, and -deformed AlxCoCrFeNi ($0 \le x \le 2$) high-entropy alloys. Journal of Alloys and Compounds 488 (2009) 57–64

[7] W.R. Wang, W.L. Wang, S.C. Wang, Y.C. Tsai, C.H. Lai, J.W. Yeh. Effects of Al addition on the microstructure and mechanical property of AlxCoCrFeNi high-entropy alloys. Intermetallics 26 (2012) 44-51.

[8] J. Joseph, T. Jarvis, X.H. Wu, N. Stanford, P. Hodgson, D.M. Fabijanic. Comparative

[9] T.F. Yang, S.Q. Xia, S. Liu, C.X. Wang, S.S. Liu, Y. Zhang, J.M. Xue, S. Yan, Y.G. Wang. Effects of Al addition on microstructure and mechanical properties of AlxCoCrFeNi High-entropy alloy. Materials Science & Engineering A 648 (2015) 15–22.

[10] Y.Z. Shi, L. Collins, R. Feng, C. Zhang, N. Balke, P.K. Liaw, B. Yang, Homogenization ol AxCoCrFeNi high-entropy alloys with improved corrosion resistance. Corr. Sci. 133 (2018)120-131

[11] J.C. Rao, H.Y. Diao, V. Ocelík, D. Vainchtein, C. Zhang, C. Kuo, Z. Tang, W. Guo , J.D. Poplawsky, Y. Zhou, P.K. Liaw, J. Th. M. De Hosson. Secondary phases in AlxCoCrFeNi high-entropy alloys: An in-situ TEM heating study and thermodynamic appraisal. Acta Materialia 131 (2017) 206-220.

[12] H.P. Chou, Y.S. Chang, S.K. Chen, J.W. Yeh, Microstructure, thermophysical an electrical properties in AlxCoCrFeNi ($0 \leq x \leq 2$) high-entropy alloys, Mater. Sci. Eng. B 163 (2009) 184-189.

[13] J. Wang, S.Z. Niu, T. Guo, H.C. Kou, J.S. Li. The FCC to BCC phase transformation kinetics in an Al0.5CoCrFeNi high entropy alloy. Journal of Alloys and Compounds 710 (2017) 144-150.

[14] S. Uporov, V. Bykov, S. Pryanichnikov, A. Shubin, N. Uporova. Effect of synthesis route on structure and properties of AlCoCrFeNi high-entropy alloy. Intermetallics 83 (2017) 1-8.

[15] Y.K. Lv, Ruyi Hu, Zhihao Yao, Jian Chen, Dapeng Xu, Yong Liu, Xinhui Fan, Cooling rate effect on micro-structure and mechanical properties of Alx CoCrFeNi high entropy alloys, Mater. Design 132 (2017) 392-399.

[16] F.J. Wang, Y. Zhang, G.L. Chen, H.A. Davies, Cooling Rate and Size Effect on the Microstructure and Mechanical Properties of AlCoCrFeNi High Entropy Alloy. J. Eng. Mater. Technol 131(3), (2009) 034501.

[17] W. Ji, Z.Y. Fu, W.M. Wang, H. Wang, J.Y. Zhang, Y.C. Wang, F. Zhang,
Mechanical alloying synthesis and spark plasma sintering consolidation of CoCrFeNiAl high-entropy alloy. Journal of Alloys and Compounds 589 (2014) 61–66.

[18] H.R. Sistla, J.W. Newkirk, F.F. Liou, Effect of A/Ni ratio, heat treatment on phase transformations and microstructure of AlxFeCoCrNi2-x (x=0.3, 1) high entropy alloys. Mater. Design 81 (2015)113-121.

[19] J. Cieslak, J. Tobola, K. Berent, M. Marciszko, Phase composition of AlxFeNiCrCo high entropy alloys prepared by sintering and arc-melting methods, J. Alloys Compd. 740 (2018) 264-272.

[20] W.R. Wang, W.L. Wang, J.W. Yeh. Phases, microstructure and mechanical properties of AlxCoCrFeNi high-entropy alloys at elevated temperatures. Journal of Alloys and

[21] K. Jasiewicz, J. Cieslak, S. Kaprzyj, J. Tobola. Relative crystal stability of AlxFeNiCrCo high entropy alloys from XRD analysis and formation energy calculation, J. Alloys Compd. 648 (2015) 307-312

[22] C. Zhang, F. Zhang, H.Y. Diao, M.C. Gao, Z. Tang, J.D. Poplawsky, P.K. Liaw. Understanding phase stability of Al-Co-Cr-Fe-Ni high entropy alloys. Materials and Design 109 (2016) 425–433.

[23] J.E. Saal, I.S. Berglund, J.T. Sebastian, P.K. Liaw, G.B. Olson. Equilibrium high entropy alloy phase stability from experiments and thermodynamic modeling.
Sripta Mater. 146 (2018) 5-8.

[24] K. Jasiewicz, S. Kaprzyk, J. Tobola, Interplay of crystal structure preference and magnetic ordering in high entropy CrCoFeNiAl alloys, Acta Phys. Pol. A 133 (2018) 511

[25] J. Rodriguez-Carvajal, Recent advances in magnetic structure determination by neutron powder diffraction, Physica B 192 (1993) 55.

[26] T. Stopa, S. Kaprzyk, J. Tobola, Linear aspects of the Korringa-Kohn-Rostoker formalism, J. Phys. Condens. Matter., 16 (2004) 4921

[27] A. Bansil, S. Kaprzyk, P.E. Mijnarends, J. Tobola, Electronic structure and magnetism of Fe3-xVxX (X= Si, Ga, and Al) alloys by the KKR-CPA method, Phys. Rev. B, 60 (1999) 13396

[28] J. P. Perdew and Y. Wang, Accurate and simple analytic representation of the electron-gas correlation energy, Phys. Rev. B 45 (1992) 13244

[29] S. Kaprzyk and A. Bansil, Green's function and a generalized Lloyd formula for the density of states in disordered muffin-tin alloys, Phys. Rev. B 42, 7358.

[30] J. Cieslak, J. Tobola, S.M. Dubiel. Site occupancies in sigma-phase Fe–Cr–X (X = Co, Ni) alloys: Calculations versus experiment, Computational Materials Science 122 (2016) 229–239

[31] Q. Hou, R. Mutharasan, M. Koczak, Feasibility of aluminium nitride formation in aluminum alloys, Materials Science and Engineering A195 (1995) 121-129

[32] D. Vempaire, S. Miraglia, J. Pelletier, D. Fruchart, E.K. Hlil, L. Ortega, A. Sulpice, F. Fettar. Structural and magnetic properties of Ni3N synthesized by multidipolar microwave plasma-assisted reactive sputtering, Journal of Alloys and Compounds 480 (2009) 225–229.

[33] Y.B. Zhao, X.H. Peng, T. Fu, C. Huang, H.G. Xiang, N. Hu, C. Yan. Investigation of mechanical behaviour of amorphous aluminium nitride, Materialia 2 (2018) 148–156.

[34] B.D. Leskiw, A.W. Castleman Jr, C.Ashman and S.N. Khanna; Reactivity and electronic

[35] L. Guo, H.-S. Wu, Z.-H. Jin, First-principles investigation of structure and stability of AlnNm clusters, Inter. J. Quantum Chem. 103 (2005) 291-298.

Two series of $Cr_xAlFeCoNi$ HEA were fabricated, their properties were compared

Two crystalline *bcc* phases cannot be separated using standard XRD technique

Bcc-grey and σ phases have very close chemical compositions

For sintered samples high-temperature nitrogen corrosion was observed

Highly selective corrosion resulted in Al_nN_m–phases and Al-depleted HEA